Transient Absorption Spectroscopy Studies of CdTe-cationic meso-tetrakis(4-N-methylpyridyl) zinc porphyrin ($ZnTMPyP_4$)

Contact *igounko@tcd.ie*

Shane Gallagher
School of Chemistry and CRANN,
Trinity College Dublin, Dublin 2, Ireland

John M. Kelly,
School of Chemistry, Trinity College Dublin,
Dublin 2, Ireland

Yurii K. Gun'ko
School of Chemistry and CRANN,
Trinity College Dublin, Dublin 2, Ireland

Páraic M. Keane
School of Chemistry and Chemical Biology,
University College Dublin, Dublin, Ireland

Luis M. Magno
School of Chemistry and Chemical Biology,
University College Dublin, Dublin, Ireland

Susan J. Quinn
School of Chemistry and Chemical Biology,
University College Dublin, Dublin, Ireland

Introduction

Quantum dots (QDs) are fluorescent semiconductor (e.g. II-VI) nanocrystals, which have attracted enormous interest due to their unique photophysical properties and range of potential applications in photonics and biochemistry [1]. This is largely due to the fact that their emission is tunable to a desired energy by controlling particle size, size distribution and composition of the nanocrystals. Our aims are to develop new QD based surface sensitive probes for a number of applications including biochemical sensing. Previously we have demonstrated that functionalisation of QDs enables the delivery of the particles into cells, allowing the targeting of specific components [2]. We have also reported the preparation of chiral quantum dots of II-VI semiconductors [3], which can potentially open new horizons in enantiomeric sensing and specific targeted intracellular delivery of nanoparticles. The development of this research area necessitates a thorough understanding of the electronic processes governing light emission and in particular the properties of the exciton (electron-hole pair) and defect excited states of the functionalized QDs in aqueous solution. Of key importance here is the fact that multiphoton effects are observed unless measurements are performed at very low energy (< 50 nJ). The ULTRA equipment is ideally appropriate technique for these measurements.

In this work using the ULTRA equipment we have investigated transient behaviour of a TGA capped CdTe -cationic meso-tetrakis(4-N-methylpyridyl) zinc porphyrin (ZnTMPyP4), see Figure 1.

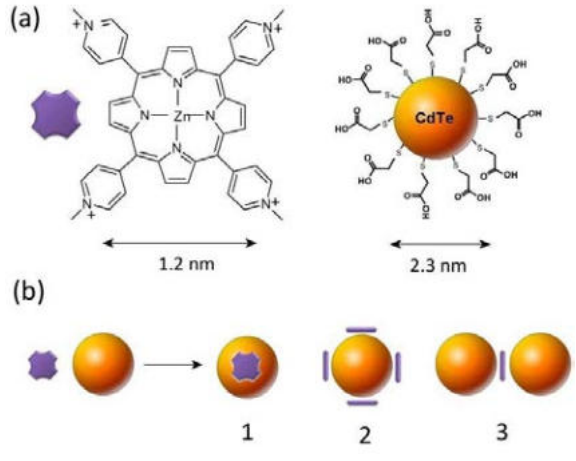

Figure 1. Schematic presentation of ZnTMPyP4 - CdTe QD system.

2. Studies of CdTe-cationic meso-tetrakis(4-N-methylpyridyl) zinc porphyrin (ZnTMPyP4)

The absorption and emission spectra of the two components, ZnTMPyP4 and 2.3 nm CdTe, are given in Figure 2. At neutral pH the absorption spectrum of the ZnTMPyP4 is dominated by the intense and characteristic Soret band at 436 nm with two weaker Q-bands also present at 564 and 608 nm. Excitation of the porphyrin at 400 nm results in strong singlet emission between 600 and 750 nm (maximum at 632 nm).

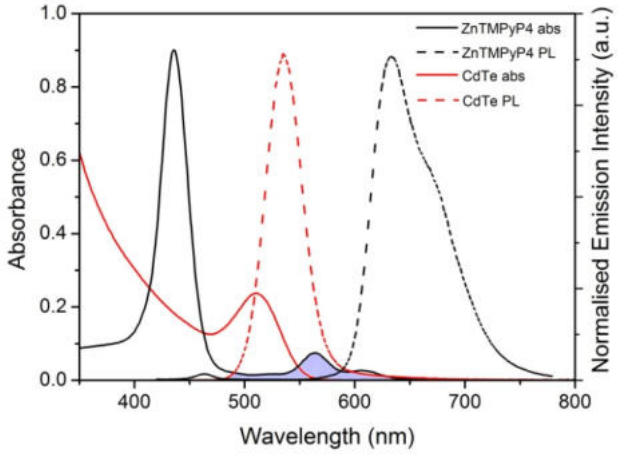

Figure2. Comparison of the absorption spectra of equimolar concentrations of ZnTMPyP4 and CdTe (4.4 μM) in Millipore water and normalised emission spectra recorded upon excitation at 400 nm (note emission quantum yield for CdTe is approx. ten times greater than that of ZnTMPyP4).

Titration of CdTe QDs to a solution of ZnTMPyP4, (4.4 μM in Millipore water) resulted in a shift in the Soret band at 436 nm to 444 nm, which was accompanied by a dramatic decrease (>40%) in the absorbance. In addition, the Q-bands were found to shift from 564 and 608 nm to 573 and 616 nm respectively. The shift in the Q-band position is typically taken as an indication of strong electronic coupling. Interestingly, the changes in the porphyrin spectrum appear to reach completion upon addition of 0.25 equivalents of QDs (Figure 3). Between 0 and 0.25 equivalents of QDs a clear isosbestic point is observed at 448 nm. Addition of the CdTe QDs to porphyrin in H_2O results in a marked red-shift and hypochromism in the

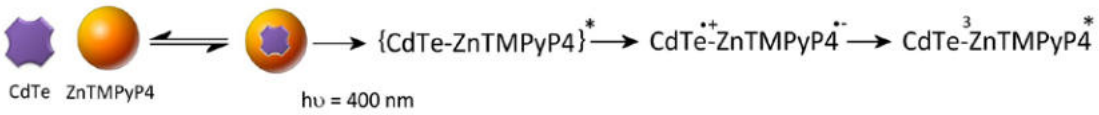

Scheme 1. The possible excited-state deactivation pathways for the CdTe-ZnTMPyP4 system.

porphyrin absorption spectrum, that is indicative of a non-covalent binding interaction with the QD surface. Low equivalents of the quantum dot were required for complete quenching of the porphyrin fluorescence revealing that one quantum dot may quench more than one porphyrin (Figure 4).

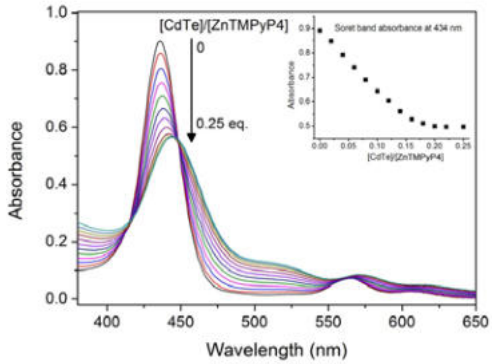

Figure 3. UV/vis absorption spectra of 4.4 μM ZnTMPyP4 in the presence of increasing concentrations of CdTe. Inset: absorption at 434 nm plotted against CdTe equivalents.

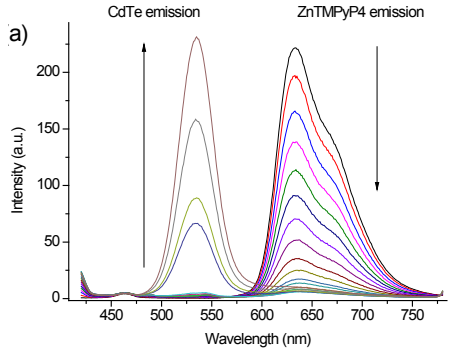

Figure 4. Fluorescence spectra of 4.4 μM ZnTMPyP$_4$ in presence of increasing CdTe (0-2.64 μM), λ_{exc} =400 nm.

Similarly addition of porphyrin to the quantum dot provided evidence for very efficient quenching of the CdTe photoluminescence, suggesting the formation of CdTe-porphyrin aggregates. Definitive evidence for such aggregates was gathered using small angle X-ray spectroscopy (SAXS).

Excitation of a 2:1 CdTe-TGA:ZnTMPyP4 sample with low energy 400 nm 150 ps pulses induces instantaneous bleaching of the CdTe exciton band at 510 nm. This is then followed by a rapid recovery (1.3 ps; 10 ps) of the absorption in this spectral region. Concurrently the Soret band of the bound porphyrin (at 445 nm) is bleached (τ = 1.3 ps), giving rise to a long-lived (τ> 3ns) species (Figure 5).

While energy transfer is possible, no fluorescence from the porphyrin is observed. This either means energy transfer does not occur or that an alternative quenching process takes place. After consideration of the various possible energy and electron transfer processes, we propose that photo-excitation of the CdTe-ZnTMPyP4 conjugate is followed by very rapid electron transfer from the quantum dot to the porphyrin. This is followed very rapidly by a reverse electron transfer yielding the triplet state of the bound porphyrin (Scheme 1).

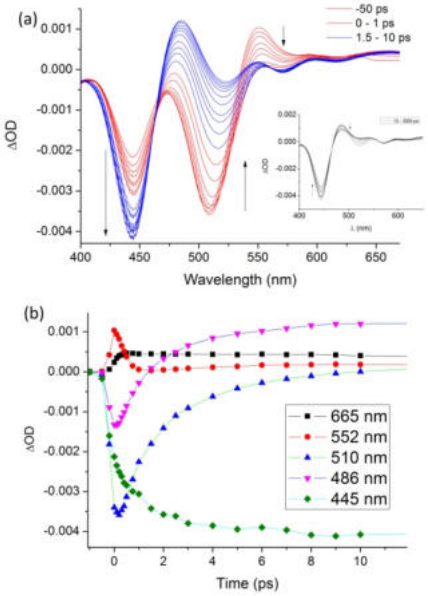

Figure 5. (a) ps-TA spectrum of 2:1 CdTe-TGA:ZnTMPyP4 up to 10 ps after pump pulse. Inset: spectra at longer time delays up to 3 ns. (b) Kinetics at short times.

3. Conclusions

The photophysical behaviour of a new donor-acceptor system comprising a ZnTMPyP4 porphyrin and CdTe QD has been studied in detail. The transient absorption measurements carried out under conditions, where only single photon excitation occurs, reveal ultrafast processes consistent with very rapid electron transfer and formation of the porphyrin triplet state. Further experiments to confirm this will require transient monitoring in the 800-1000 nm region and we would hope to carry out such experiments in the near future.

We believe that this research will be very useful for further development of new QD systems with controlled photophysical characteristics for a range of potential applications.

Acknowledgements

We acknowledge financial support from Science Foundation Ireland (grant SFI 07/IN.1/I1862 RFP/007/CHEF437 and the EU for funded access to STFC (App 1110017).

References

1. (a). P. Alivisatos, Nature Biotechnol.2004, **22**, 47; (b) T. M. Jovin, ibid. 2004, **21**,32.

2. (a) S. J. Byrne et al., *J. Mater. Chem.*, 2006, **16**, 2896; (b) S. J. Byrne et al. *ChemMedChem.,* 2007, 2, 183; (c) S. J. Byrne, et al., *Small*, 2007, **3**, 1152.

3. (a) M. P. Moloney et al. *Chem. Comm.*, 2007, 3900; (b) S. D. Elliott,et al., *Nano lett* , 2008, **8**, 2452; (c) J. E. Govan et al., , *Chem. Comm*, 2010, **46**, 6072. (d) S. Gallagher et al., *J. Mater. Chem,* 2010, **20**, 8350 – 8355. (e) M. Wojdyla, S. A. Gallagher, M.P. Moloney, Y. K. Gun'ko, J M. Kelly, Luis M. Magno, Susan J. Quinn, I. P. Clark, G. M. Greetham, and M. Towrie, *J. Phys Chem. C.,*2012, dx.doi.org/10.1021/jp3023088.

Human Epidermal Growth Factor Receptor (EGFR) Aligned on the Plasma Membrane Adopts Key Features of Drosophila Asymmetry

Contact *C.Tynan@stfc.ac.uk*

Chris J. Tynan
Central Laser Facility
Rutherford Appleton Laboratory

Selene K. Roberts
Central Laser Facility

Martyn Winn
CSE Department
Daresbury Laboratory

Daniel J. Rolfe
Central Laser Facility
Rutherford Appleton Laboratory

David T. Clarke
Central Laser Facility
Rutherford Appleton Laboratory

Hannes Loeffler
CSE Department
Daresbury Laboratory

Marisa Martin-Fernandez
Central Laser Facility
Rutherford Appleton Laboratory

Introduction

The human epithelial growth factor receptor (hEGFR; aka HER1) is the founding member of the growth factor receptor tyrosine kinase (RTK) super-family. This family also comprises 18 sub-groups of cell surface receptors for many growth factors, cytokines and hormones [1]. The EGFR family has evolved from one receptor/one ligand in C. elegans, through one receptor/multiple ligands in flies, to a family comprising four receptors (HER1 and ErbB2-4, known as HER2-4 in humans) and 13 extracellular ligands in mammals [2]. The EGFR family are key regulators of cell-to-cell inductive processes and cell fate [3]. Their function is to transmit growth factor signals from the outside to the inside of the cell where changes in gene expression allow the cell to respond to the new circumstances. Deregulated signalling by cell surface HER1 receptors (e.g. via activating mutations in the HER1 gene) is implicated in a substantial percentage of lung cancers [4]. As activation of these receptors has been shown to result in the growth and progression of the malignancy, there have been considerable research efforts directed toward the development of effective inhibitors of HER1. Several of these cancer drugs are in different stages of pre-clinical and clinical trials [5].

The structure of the extracellular domain of the HER1
Crystallographic studies of HER1 ectodomain fragments bound to two types of ligands, epidermal growth factor (EGF) and transforming growth factor alpha (TGFα), have shown quasi-a symmetric 2:2 ligand-receptor dimers [14, 15]. Unliganded HER1 monomers are held in a closed conformation by an intramolecular tether formed by loops in subdomains II and IV [16-18]. The data suggest that ligand binding and dimerisation involves major extracellular structural rearrangements in HER1 because in ligand-occupied receptor dimers the intramolecular tether is broken and the receptor is opened into an extended conformation which interacts with another monomer to form a back-to-back dimer [14, 15, 19].

The original paradigm proposed for the RTKs was that the ligand induced the dimerization of monomeric unliganded receptors via ligand-crosslinking of two receptor moieties [1]. Contrary to these expectations, HER1dimer structures showed that receptor dimerisation was not directly mediated by the binding of ligand but achieved exclusively via receptor-receptor contacts, suggesting a mechanism for how unliganded receptor monomers are maintained in an 'autoinhibited' configuration.

The typical representation of the holoreceptor has been derived by putting together the available crystal structures of extracellular fragments and intracellular fragments [7-9, 14-16, 19]. In this model, the extracellular domains are oriented with respect to the membrane based on the historical view that receptors are protruding from the plasma membrane as antennae.

Insights into signalling by the HER1 receptor

The primary structure of HER1 is shared by all receptor tyrosine kinases and consists of a single polypeptide chain (1,186 amino acids) of 170 kD, containing a heavily glycosylated 622-amino acid residue amino-terminal extracellular ligand binding domain that is connected to the cytoplasmic domain by a single transmembrane (TM) helix of 23 residues. The 542-residue cytoplasmic domain contains a conserved 250-amino acid tyrosine kinase core [6]. Ligand binding induces the dimerisation of HER1 ectodomains. This leads to the formation of an asymmetric dimer by the two associated intracellular kinases [7], that is stabilised by the inner juxtamembrane (JM) region [8, 9]. In the ligand-mediated kinase dimer, kinase activation proceeds though an allosteric mechanism in which the C-lobe of one kinase "pushes" the N-lobe of the other kinase towards the active site in an interaction that is highly reminiscent of the activation of CDK2 by binding of cyclinA [10]. Active kinases then proceed to phosphorylate tyrosine residues in the 229-residue carboxy-terminal tail of the receptor [7], which when posphorylated act as docking sites for a large repertoire of adapters and enzymes containing Src homology 2 (SH2) domains [11]. These include, for example Grb2, GAP, Shc, phospholipase Cγ(PLCγ), and phosphatidylinositol 3'-kinase (PI3K) , which regulate Ras/Rho-like GTPases, Ca2+ second messenger production, and the Ras-activated MAP/SAP kinase pathways [12] leading to cell proliferation, changes in cell morphology, trafficking, and the termination of signals via endocytosis of the receptor-ligand complexes [13].

Ligand-membrane distances as reporters of protein conformation

Protein conformation at the plasma membrane can be investigated from the distance from a specific site in the protein (e.g. the binding site of a cognate ligand) to the cell surface. This distance can be determined from the variation of the efficiency of Förster resonance energy transfer (FRET) between fluorescent donors labelling the protein and acceptors labelling the surface, measured as a function of acceptor surface density. FRET is a phenomenon by which the excited-state energy of an optically excited fluorescent molecule (donor) is transferred to a

neighbouring fluorescent molecule molecule (acceptor) non-radiatively via intermolecular dipole coupling [28]. FRET between donors and acceptors occurs when the electronic levels of these different molecules overlap. Being a dipole-dipole interaction, FRET is extremely sensitive to short intermolecular distances (<10 nm).

Analytical expressions describing the energy transfer process between random distributions of donors (e.g. in specific sites in proteins) and acceptors on lipid membrane surfaces have been derived for a number of geometries (see for example [28]]. The solutions to these equations are the distance of closest approach between the protein-bound fluorescent donor probe and a lipid acceptor chromophore at the plasma membrane. Examples of work using this FRET method include an investigation to derive the mean distance between the EGF binding site of HER1 and the plasma membrane of cells in suspension [29], to derive changes in conformation of α4-Integrin during activation [30], and to determine the minimum separation between the protein portion of GPI-anchored proteins to the bilayer surface [31]

HER1 aligned on the membrane adopts key features of drosophila EGFR asymmetry

To investigate the relevance of the MD-derived asymmetric model of the HER1 dimer [33] to EGF-binding heterogeneity (and/or the previously suggested negative cooperativity [26]), Tynan et al extended a FLIM -FRET assay previously reported to include FRET titrations as a function of acceptor concentration together with a data analysis method based on Monte Carlo simulations [34]. This combination allowed full quantification of the distance of closest approach between HER1-bound ligands and the surface of adherent epithelial cells, the assessment of the variation associated to the distance measurement, and also the rejection of potential sources of artifacts which can be inherent in standard flow cytometry (non-imaging) FRET measurements (e.g., photobleaching, nonradiative transfer, and nonuniform distributions of FRET donors and acceptors).

Given the known flexibility regions in the accepted crystallographic HER1 ectodomain dimer structure, the FRET-derived distance data obtained from HER1 that display high-affinity for EGF could only be reconciled with these structural data if receptors are aligned flat on the membrane (Fig. 1). MD simulations of doubly-liganded, singly-liganded and unliganded HER1 dimers aligned on a model membrane under the same conditions revealed that the asymmetry resulting from alignment on the membrane shares a number of key features with the equivalent doubly-liganded and singly-liganded structures observed recently in soluble dEGFR [27]. These results suggest that the structural basis for negative cooperativity is conserved from invertebrates to humans but that in HER1 the extracellular region asymmetry requires interactions with the plasma membrane.

Concluding remarks

FRET is commonly used at the ensemble and single molecule levels to investigate interactions between protein species (see for example [35-37]. Although less frequently employed, FRET can also be used to investigate the conformation of membrane proteins in the plasma membrane. This is derived by measuring FRET in a 2-dimensional geometry, i.e. between a plane of donor-labelled protein sites and a plane of lipid acceptors in the membrane, which allow the derivation of distances of closest approach. In cases where high-resolution structures are also available, this FRET method in combination with computational approaches (e.g. Monte Carlo simulations to derive distances of closest approach and MD simulations to relax structures in the membrane) can reveal which protein conformations are best consistent with the experimentally derived FRET-derived distances. Such an approach has very recently revealed a new conformation of HER1 in which in the ectodomain of the dimer is aligned in contact with the plasma membrane [34]. Interestingly, this conformation suggests that the structural basis for negative cooperativity is conserved from invertebrates to humans, solving a 30-year old puzzle in EGFR research.

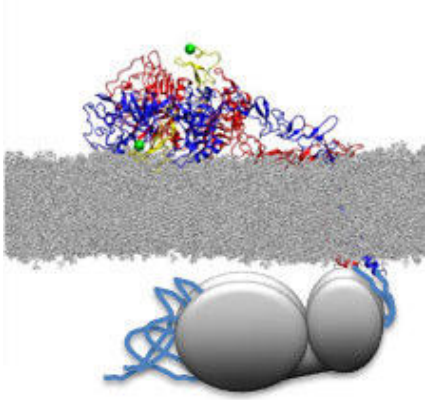

Fig. 1. Cartoon of HER1 holoreceptor combining a HER1 ectodomain dimer with two bound ligands, modelled on crystallographic structures [14-16] and placed in the membrane using MD simulations [33]. Green spheres indicate the N termini of the ligands to which donor dyes are attached. The orientation of the intracellular domain is based on electron microscopy data [39].

References

1. Schlessinger, J. (2000) Cell. 103, 211-225. **2**. Yarden, Y. and Sliwkowski, M. X. (2001) Nat Rev Mol Cell Biol. 2, 127-137. **3.** Downward, J., Parker, P. and Waterfield, M. D. (1984). Nature. 311, 483-485. **4**. Paez, J. G., et al (2004). Science. 304, 1497-1500. **5**. Jackman, D. M., et al. (2009) Clinical Cancer Research. 15, 5267-5273. **6.** Ullrich, A. et al. (1984) Nature. 309, 418-425. **7.** Zhang, X. W., Gureasko, J., Shen, K., Cole, P. A. and Kuriyan, J. (2006) Cell. 125, 1137-1149. **8**. Brewer, M. et al (2009) Mol Cell. 34, 641-651. **9** . Jura, N., et al. (2009) Cell. 137, 1293-1307. **10.** Jeffrey, P. D et al (1995) Nature. 376, 313-320. **11**. Pawson, T. (2004) Cell. 116, 191-203. **12**. Zhang, W. and Liu, H. T. (2002) Cell Research. 12, 9-18. **13**. Carpenter, G. (2000) Bioessays. 22, 697-707. **14.** Garrett, T. P. et al (2002) Cell. 110, 763-773. **15.** Ogiso, H et al (2002) Cell. 110, 775-787. **16**. Ferguson, K. M et al (2003) Mol Cell. 11, 507-517. **17.** Bouyain, S et al (2005) Proc Natl Acad Sci U S A. 102, 15024-15029. **18.** Hyun-Soo, C. and Leahy, D. J. (2002) Science. 297, 1330-1333. **19.** Burgess, A. W et al (2003) Mol Cell. 12, 541-552. **20**. Magun, B. E., et al (1980) Journal of Biological Chemistry. 255, 6373-638. 21. Shoyab, M et al (1979) Nature. 279, 387-391. **22.** Ullrich, A. et al Cell. 61, 203-212. **23.** Defize, L. H. K et al (1989) Journal of Cell Biology. 109, 2495-2507. **24.** Friedman, B. A et al (1984) PNAS. 81, 3034-3038. **25.** Mattoon, D., Klein, P., Lemmon, M. A., Lax, I. and Schlessinger, J. (2004) Proc Natl Acad Sci U S A. 101, 923-928. **26.** Macdonald, J. L. and Pike, L. J. (2008) Proc Natl Acad Sci U S A. 105, 112-117. **27.** Alvarado, D., et al (2010) Cell. 142, 568-579. **28.** Stryer, L. and Haugland, R. P. (1967) Proc Natl Acad Sci U S A. 58, 719-726. **29.** Carraway, K. L., et al (1990) Biochemistry. 29, 8741-8747. **30.** Chigaev, A., et al (2003) Biophys J. 85, 3951-3962. **31.** Lehto, M. T. and Sharom, F. J. (2002) Biochemistry. 41, 8368-8376. **32.** Webb, S. E. D et al (2008) Biophys J. 94, 808-819. **33.** Kastner, J., (2009) J Struct Biol. 167, 117-128. **34** . Tynan, C. J. (2011) Mol Cell Biol. 31, 2241-2252. **35.** Martin-Fernandez, M., et al (2002). Biophys J. 82, 2415-2427. **36.** Webb, S. E et al (2008) Opt Express. 16, 20258-20265. **37.** Webb, S. E. D. (2006) Opt. Lett. 31, 2157-2159. **38** . Wolber, P. K. and Hudson, B. S. (1979) Biophys J. 28, 197-210. **39.** van Bueren, J. J. L. et al, (2008) Proc Natl Acad Sci U S A. 105, 6109-6114

Probing the Mechanism of Blue Light Sensing BLUF Domain Proteins: A Study Through Transient Infra-red Spectroscopy and Unnatural Amino Acid Incorporation

Contact *s.meech@uea.ac.uk*

Richard Brust
Stony Brook University
New York 11794-3400, USA

Allison Haigney
Stony Brook University
New York 11794-3400, USA

Andras Lukacs
University of Pec
H-7624 Pécs, Hungary

Kiri Addison
University of East Anglia
Norwich NR4 7TJ

Rui-Kun Zhao
University of East Anglia
Norwich NR4 7TJ

Gregory M. Greetham
Research Complex at Harwell
Central Laser Facility

Michael Towrie
Research Complex at Harwell
Central Laser Facility

Peter J. Tonge
Stony Brook University
New York 11794-3400, USA

Stephen R. Meech
University of East Anglia
Norwich NR4 7TJ

Introduction

Flavoproteins are a large family of proteins that contain a covalently or non-covalently bound flavin cofactor[1]. Although the isoalloxazine ring of the flavin functions predominantly as an electron transfer intermediate in biochemical oxidation-reduction reactions, there are at least three subfamilies of flavoproteins that function as photoreceptors: the light-oxygen-voltage (LOV) domain proteins, the cryptochromes, and the Blue Light Using FAD (BLUF)-domain proteins[2]. The chromophores in traditional photoreceptors such as the rhodopsins, xanthopsins and phytochromes undergo an isomerization when light is absorbed. However, this is not the case for flavoprotein receptors. Consequently there is substantial interest in understanding how absorption of light by the flavin is coupled to the conformational change(s) that lead to the signaling state.

AppA is the first and best characterized BLUF domain photoreceptor and is found in *Rhodobacter sphaeroides* where it acts as an antirepressor of photosystem biosynthesis. In the dark AppA binds PpsR, a transcription factor, forming an AppA-$PpsR_2$ complex. When irradiated with high intensity blue light, the complex dissociates releasing PpsR and enabling PpsR to bind to DNA and repress photosystem biosynthesis. Photoexcitation of AppA with 450 nm light shows a 10 nm red shifted absorption spectrum of the flavin in the signaling state and is known to involve an increase in the hydrogen bonding to the flavin C4=O from the protein[4]. The dark state recovers on a time scale of tens of minutes. However, the mechanism leading to these structural changes and how they relate to BLUF domain activity remain to be fully elucidated. We have shown that the protein matrix responds instantaneously (<100 fs) to blue light, where a mechanism involving keto-enol tautomerisation of a glutamine side chain was invoked (Q63) [5]. Here we probe this mechanism further using non-natural amino acids (fluorotyrosine analogues).

A new direction involves *Acinetobacter baumannii*, a gram-negative opportunistic pathogen that poses a significant threat to human health due to its resistance to many frontline antibiotics and ability to survive in harsh environments. In particular, the ability of *A. baumannii* to form biofilms has been attributed to the bacteria's ability to survive nutrient depletion and sterilization in hospitals. It has been discovered that *A. baumannii* can sense and respond to light, and that biofilm formation is abolished in the presence of blue light, while virulence toward eukaryotic cells is enhanced. The ability to sense blue light is a result of encoding for a BLUF domain, called blsA (blue light sensing A). We probe the operation of this BLUF domain by ultrafast IR spectroscopy.

Fluorotyrosine Incorporation

Fluorotyrosine has been used as probe to study the mechanism of electron transfer in numerous systems including photosystem II, GFP and ribonucleotide reductase. The fluorinated derivatives alter both the pK_a and the redox potential of the tyrosine with minor perturbation to the protein structure. The degree to which these two parameters are modified depends on the substitution pattern. Modulating the pK_a and potential of Y21 in AppA, the tyrosine adjacent to the flavin, will enable us to unravel the interplay between proton transfer (or hydrogen bond breaking) and electron transfer. Incorporation of fluorotyrosines has commonly been used to determine whether proton coupled electron transfer (PCET) is concerted or separate. If such a PCET mechanism proves important in AppA the incorporation of different substitution patterns will allow a degree of control over the mechanism. We have successfully generated fluorotyrosines and incorporated them specifically into Y21. These proteins have been studied using steady state and ultrafast spectroscopy. This will allow us to understand the significance of electron transfer is AppA[6].

Specific incorporation of various fluorinated tyrosines into position Y21 of AppA was completed using the photoactive Y56F $AppA_{BLUF}$ mutant. This mutant leaves Y21 as the only tyrosine residue in AppA which can then be substituted. The method makes use of expression and purification of tyrosine phenol lyase (TPL) which is a promiscuous enzyme capable of using a variety of phenols, ammonia and pyruvic acid to make tyrosine and analogs. These analogs were fed into cells grown in minimal media for fluorotyrosine incorporation into AppA. The percent incorporation was checked using MALDI mass spectroscopy. The time resolved IR (TRIR) spectra for the dark and light states of wild-type, 3FY21 and 2FY21 AppABLUF are shown in figure 1.

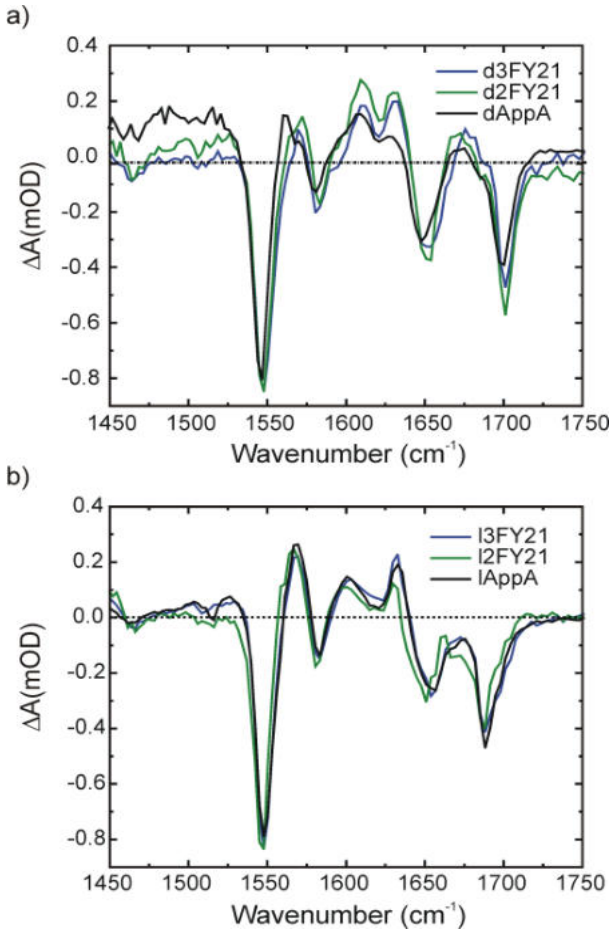

Figure 1. TRIR spectra of AppA fluorotyrosines. In dark (a) and light(b) states

These data show that the spectra of 3FY21 and 2FY21 AppABLUF are very similar to the wild-type protein, in both its dark and light adapted states, suggesting there is little or no change in the H-bond structure around the flavin due to the addition of a fluorine atom. This is consistent with the expectation that fluorinated derivatives alter the pK_a and the redox potential of the tyrosine with only minor perturbation to the structure. Therefore, we are able to discuss changes in kinetics in terms of changes in the pK_a and redox potential of the tyrosine. No significant changes were observed in the ground state recovery or excited state decay kinetics. This suggests reorganization of the protein's hydrogen bonding network that surrounds the flavin chromophore is due to direct changes in the hydrogen bonding structure caused by photoexcitation and that this process does not involve electron transfer from residue Y21.

In order to investigate the relationship between the acidity of residue Y21 with the rate of light to dark state recovery, a Brønsted analysis was used to plot the log of the rate vs. pK_a. This linear plot establishes there is a direct correlation between the pK_a of residue Y21 and the rate of light to dark state recovery, implying proton transfer must be proportional to the activation energy for light to dark recovery. In addition, the slope of the plot (termed -α) is calculated to be -0.76 suggesting the proton is almost fully transferred in the transition state. These data allow us to propose a mechanism for the light to dark state recovery of wild-type AppA (Figure 2) where proton transfer from Y21 is the rate determining step in the recovery. After the formation of lAppA, residue Q63 tautomerizes so that the side chain deprotonated alcohol remains hydrogen bonded to the hydroxyl side chain of Y21. This enol conformation of Q63 allows the glutamine to act as a base and abstract a proton from residue Y21. After protonation of the enol, Q63 will rotate thus breaking the hydrogen bond to the C4=O of the flavin and

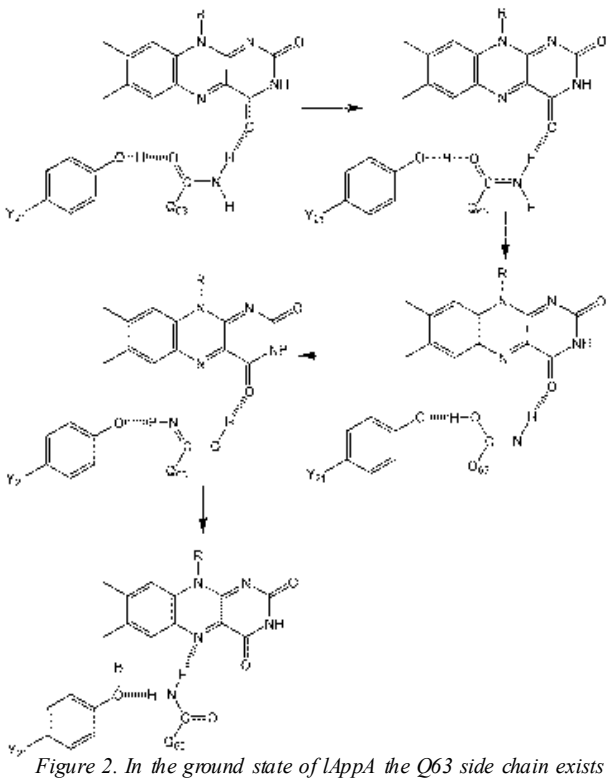

Figure 2. In the ground state of lAppA the Q63 side chain exists as an equilibrium mixture of keto and enol tautomers.

form a new hydrogen bond with the flavin N5 atom. The last step involves a second tautomerization to return to the more stable keto state of Q63. Residue Y21 will now be solvent accessible and able to abstract a proton from the solvent. Abstraction of the proton from Y21 by Q63 is the rate determining step of the light to dark recovery. This mechanism also explains the observed normal isotope effect in deuterated buffer. In the enol tautomer there is a hydrogen bond between Q63 and the Y21 that is essential for stabilization of lAppA. Upon recovery the enol tautomer, will abstract a hydrogen from residue Y21 in the rate determining step of relaxation back to the dark state. This tautomer will then rotate breaking the hydrogen bond with the C4=O of the flavin and form a new hydrogen bond with the N5 atom of the flavin. This rotated state of Q63 will then return to the more stable keto form and Y21 will abstract a proton from the solvent.

Ultrafast dynamics of blsA

Similar to other BLUF proteins, photoactivation of dark adapted blsA (dblsA) results in a 12 nm red shift in the flavin absorption band at 459 nm upon formation of the light activated state (lblsA). lblsA relaxes back to dblsA with a half-life of 9 min which is similar to that of the well characterized BLUF protein AppA ($t_{1/2}$ 15 min). To investigate structural similarities and differences between blsA and AppA, we used ultrafast time resolved IR (TRIR) spectroscopy to probe the primary structural changes associated with photoexcitation of dblsA. The TRIR method reported evolution of the pump-on minus pump-off transient difference spectra following excitation of the flavin chromophore with a 100 fs visible pulse. The resulting spectra are shown in figure 3. With the exception of a new bleach at 1670 cm^{-1} in the TRIR spectrum of lblsA, key flavin modes in the 1500-1620 cm^{-1} region as well as the environmentally sensitive C4=O carbonyl mode at 1700 $cm^{-1}$are present at the same positions as those observed for AppA. The 1700 cm^{-1} band in dblsA shifts to ~1685 cm^{-1} in lblsA, indicative of an increase in hydrogen bond strength between the flavin C4=O group and a conserved glutamine that is a component of the hydrogen network surrounding the chromophore. This change in hydrogen bonding is an early structural event that ultimately

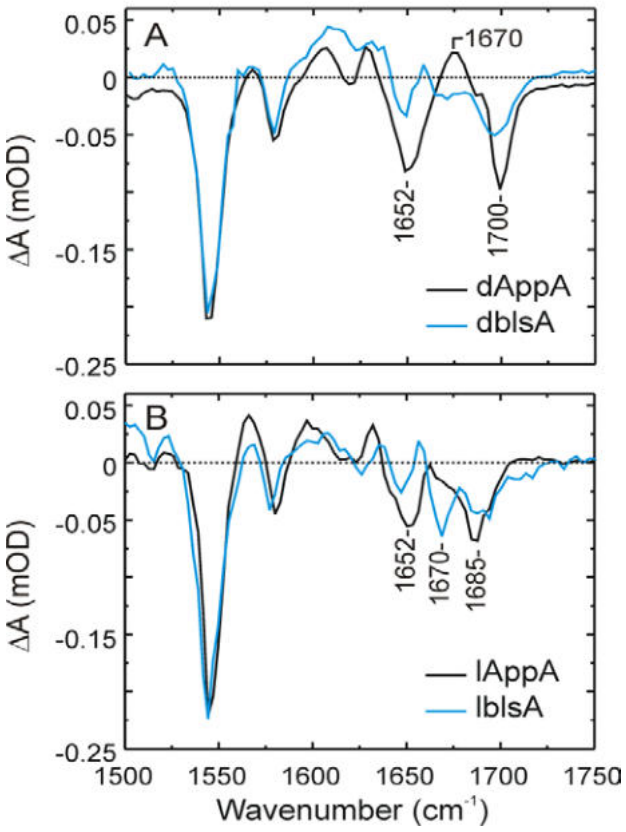

Figure 3. TRIR spectra of AppA (black) and blsA (blue) taken 3 ps post excitation. A. TRIR of dark adapted proteins. B. TRIR of photoactivated proteins.

leads to the signaling state of the BLUF proteins. Ground state recovery kinetics were measured for d and lblsA, revealing biexponential kinetics similar to that of AppA. Taken together, these data suggest that the ground states of both the dark and light adapted states of AppA and blsA are broadly similar. A key feature in the TRIR of dAppA is the transient (positive ΔA) at 1670 cm^{-1} that is absent in free flavin, lAppA and photoinactive mutants of AppA, and that has been tentatively assigned to the amide side chain of Q63[4]. However, uniquely for a photoactive BLUF protein, in dblsA the 1670 cm^{-1} transient is absent or obscured while a bleach is observed at this position in lblsA. We speculate that this new bleach is also present in dblsA where it cancels out the transient observed in dAppA. To provide additional information on the structural change accompanying light state formation, we measured the light minus dark steady state FTIR difference spectrum of blsA and compared it to the analogous spectrum obtained for AppA. Both spectra exhibit the 1700(-)/1687(+) cm^{-1} difference band assigned to changes in hydrogen bonding to the flavin C4=O associated with rotation of Q51 (Q63) between dark and light states of AppA. In addition, photoexcitation also leads to formation of a 1634(5)/1620 cm^{-1} difference band in both AppA and blsA in a region where β-sheet secondary structure can be observed . Significantly, this difference mode has opposite signs in AppA 1635(+)/1620(-) cm^{-1} and blsA 1634(-)/1620(+) cm^{-1}, suggesting that the secondary structure content of dblsA resembles that of lAppA, and vice versa. In AppA the 1635(+)/1620(-) cm^{-1} difference mode has been attributed to structural rearrangement of the BLUF β-sheet, consistent with the notion that the β-strand 5 is involved in signal transduction. In AppA the N-terminal residue of β-strand 5 is a tryptophan (W104; W91 in blsA) which is hypothesized to move upon light state formation and significantly the 1635(+)/1620(-) cm^{-1} difference mode is absent in the W104A photoactive AppA mutant.

Although it is not clear how changes in β-strand 5 in AppA modulate the structure of the C-terminal domain of this protein, it is known that in the related BLUF protein PixD photoactivation leads to dissociation of PixD from the output protein PixE. PixD and AppA have similar FTIR difference spectra in the 1620-1635 cm^{-1} region, with PixD showing the characteristic 1635(+)/1620(-) cm^{-1} difference mode. We speculate that the weakening of hydrogen bonding in the β-sheet that occurs upon photoactivation in PixD is directly related to dissociation of PixE from PixD. Conversely then, the strengthening of hydrogen bonding in the blsA β-sheet upon photoactivation, revealed by the change in sign of the β-strand marker mode, supports a model for blsA photoreceptor function in which photoactivation leads to *formation* of a complex with the downstream target protein rather than dissociation[9].

Conclusions

A mechanism for light state recovery of BLUF proteins has been reported. Using unnatural amino acid incorporation in conjunction with ultrafast spectroscopy, we were able to show that the primary mechanism of light state formation does not involve proton transfer from the conserved tyrosine, but rather proton transfer is involved in dark state recovery.

Initial characterization of blsA from *Acinetobacter baumannii* has been reported. Using steady state and ultrafast vibrational spectroscopy we were able to compare the photoactivation mechanism of blsA to the BLUF photosensor AppA. Although similar photocycles are observed, vibrational data identify significant differences in β5 strand in blsA caused by photoactivation, which proposed to be directly linked to downstream signaling.

Acknowledgements

We are grateful to STFC for the award of program access to the ULTRA facility, and the staff of that facility for their assistance. SRM and PJT were supported by an NSF-EPSRC joint research grant (EPSRC EP/G002916 and NSF CHE-0822587).

References

1. A. Mattevi, Trends in Biochemical Sciences, 2006, 31, 276-283
2. A. Losi, Photochemistry and Photobiology, 2007, 83, 1283-1300
3. S. Anderson; Dragnea, V.; Masuda, S.; Ybe, J.; Moffat, K. Biochemistry 2005, 44, (22), 7998-8005
4. A. L. Stelling, K. L. Ronayne, J. Nappa, P. J. Tonge and S. R. Meech, Journal of the American Chemical Society, 2007, 129, 15556-15564
5. A. Haigney, A. Lukacs, R. K. Zhao, A. L. Stelling, R. Brust,R. R. Kim, M. Kondo, I. Clark, M. Towrie, G. M. Greetham, B. Illarionov, A. Bacher, W. Romisch-Margl, M. Fischer, S. R. Meech and P. J. Tonge, Biochemistry, 2011, 50, 1321-1328
6. McQueary, C., and Actis, L. Journal of Microbiology 2011, 49, 243-250.
7. Mussi, M. A., Gaddy, J. A., Cabruja, M., Arivett, B. A., Viale, A. M., Rasia, R., and Actis, L. A. Journal of Bacteriology 2010 192, 6336-6345..
8. A. Haigney, R.Brust, A. Lukacs, J. Jeng, E. Melief, R-K Zhao, I Clark, M. Towrie, G. Greetham, S. Meech, and P. Tonge. In Preparation.
9. R. Brust, A. Haigney, A. Lukacs, K. Addison, C-T Lai, S. Hossain, M. Towrie, G. Greetham, I. Clark, C. Simmerling, S. Meech, P. Tonge. Submitted for publication.

Vibrationally resolved chemical reaction dynamics in solution

Contact *a.orr-ewing@bris.ac.uk*

Andrew J. Orr-Ewing
University of Bristol
School of Chemistry, Bristol BS8 1TS

Stuart J. Greaves
University of Bristol
School of Chemistry, Bristol BS8 1TS

Fawzi Abou-Chahine
University of Bristol
School of Chemistry, Bristol BS8 1TS

Greg T. Dunning
University of Bristol
School of Chemistry, Bristol BS8 1TS

David R. Glowacki
University of Bristol
School of Chemistry, Bristol BS8 1TS

Gregory M. Greetham
Central Laser Facility
Rutherford Appleton Laboratory

Ian P. Clark
Central Laser Facility
Rutherford Appleton Laboratory

Michael Towrie
Central Laser Facility
Rutherford Appleton Laboratory

Introduction

Individual chemical reactions typically take place on timescales as short as femtoseconds to picoseconds. Despite these ultra-short timescales, transient intermediate species along a reaction pathway can be characterized by study of the partitioning of energy among the vibrational, rotational and translation motions of the reaction products. From numerous studies of isolated collisions in the gas phase, much has been learned about transition states and potential energy surfaces for bimolecular chemical reactions. Here, we seek to extend such studies to reactions in solution to explore how common solvents modify the energetics and dynamics. Transient broadband infra-red absorption spectroscopy with picosecond time resolution is used to determine the extent of vibrational excitation of the products of exothermic reactions, and the rate of loss of that vibrational energy to the solvent bath. Such measurements should be able to discriminate between solvent coupling to the reaction pathway *during* reactive events and solvent coupling to the reaction products *after* the reaction is complete [1-3]. The experiments also distinguish between reaction within an initial solvent cage and reaction following diffusion into the bulk solvent [4].

Three classes of chemical reaction have been successfully studied using the ultrafast IR spectroscopy capabilities of the ULTRA Facility, and illustrative outcomes are presented here.

CN radical reactions

In the gas phases, abstraction of an H atom from an organic compound RH by a CN radical to form HCN and an organic radical

$$CN + RH \rightarrow HCN + R \qquad (1)$$

produces HCN with up to 2 quanta of excitation of the C-H stretching vibration and multiple quanta of excitation of the bending mode. Our observations of such reactions in solution, with RH = cyclohexane, tetramethylsilane (TMS) and tetrahydrofuran (THF) demonstrate similar behaviour, albeit with no more than 1 quantum of C-H stretching and 2 quanta of the bending mode excited in the HCN [1,2]. Similar studies on deuterated organic compounds demonstrate formation of highly internally excited DCN products [2]. In chlorinated organic solvents, weak coupling of the HCN to the solvent means that the vibrational excitation of the products can be observed to decay over timescales as long as ~500 ps from initiation of reaction. With the aid of molecular dynamics simulations employing an accurate potential energy function for the solvated reaction, we identify two regimes of relaxation: within the initial solvent cage, as illustrated in figure 1, HCN couples its energy efficiently into the R co-product and thence to the solvent [4,5]. Following diffusion out of the solvent cage and separation of the products in the bulk liquid, any remaining excitation energy of the HCN flows more slowly into the surrounding solvent.

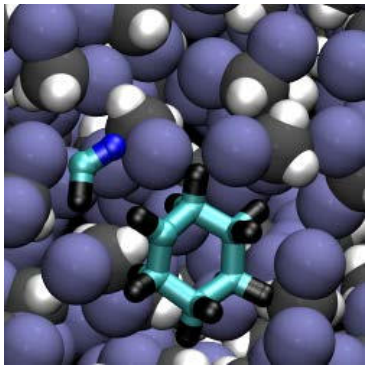

Figure 1: Snapshot from a computer simulation (by Dr D.R. Glowacki and Prof J.N. Harvey, University of Bristol) of the reaction of CN radicals with cyclohexane, showing the HCN and cyclohexyl radical products confined in close proximity within a cage of dichloromethane solvent molecules.

However, in the presence of THF, the vibrational relaxation of the nascent HCN is much more rapid because of near-resonant energy transfer to THF modes [6]. When reaction is initiated by UV photolysis of ICN dissolved in THF, the rise of HCN absorption on its fundamental bands is thus complete in ~50 ps, as shown in the time resolved spectra in figure 2 that were obtained in the region of the C-N stretching mode.

The absorptions by nascent, vibrationally excited HCN molecules are anharmonically shifted to lower wavenumber where they overlap an interfering band assigned to INC (produced by geminate recombination of I and CN), and the formation of these internally hot molecules is inferred from initial time delays in the growth of the fundamental absorption bands.

By varying the concentration of THF in solutions in $CDCl_3$ and CD_2Cl_2, and by detection of HCN using both the C-H stretching and C-N stretching fundamental bands in the IR, we

obtain a bimolecular rate coefficient for the CN + THF reaction of $1.57 \pm 0.12 \times 10^{10}$ M^{-1} s^{-1} that agrees well with the reported value for reaction of CN with ethane in the gas phase.

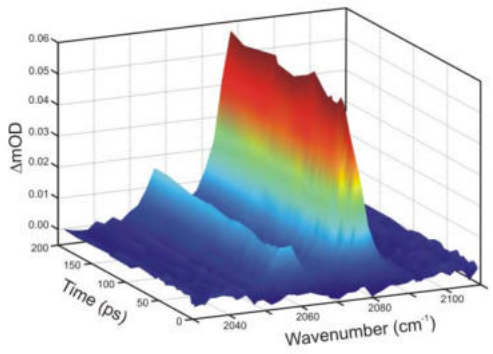

Figure 2: The growth of absorption via the C-N stretching fundamental band of HCN (centred at 2073 cm^{-1}) formed by reaction of CN with THF, following UV photolysis of ICN in solution in THF. The weaker band centred at 2052 cm^{-1} is assigned to INC which results from geminate recombination of I and CN.

Cl atom reactions

Most reactions of Cl atoms with hydrocarbons:

$$Cl + RH \rightarrow HCl + R \qquad (2)$$

are, at best, only mildly exothermic and are known from gas phase experiments not to form vibrationally excited HCl [7]. However, in selected cases, in which the radical R is resonance stabilized, giving greater exothermic energy release, HCl(v=1) can be a significant product. We have employed RH = 2,3-dimethylbut-2-ene, $(CH_3)_2C=C(CH_3)_2$ because abstraction of any one of the 12 H atoms produces a substituted allyl radical and as a result the reaction is exothermic by ~60 kJ mol^{-1}. Transient IR spectroscopy of the HCl formed from this reaction in chlorinated solvents demonstrates production of HCl(v=1) as ~20-30% of the total HCl yield, and subsequent vibrational relaxation over a period of a few hundred ps. Data for HCl formation such as those shown in figure 3 fit satisfactorily to a model in which we allow reaction of Cl atoms with the alkene both within an initial solvent cage and following diffusion into the bulk. This work is currently being prepared for publication.

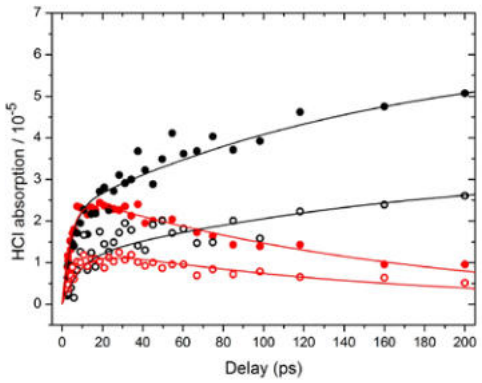

Figure 3: Time dependence of the band-integrated absorptions by HCl(v=0) (black circles) and HCl(v=1) (red circles) from reaction of Cl atoms with 2,3-dimethylbut-2-ene in solution in $CDCl_3$. Filled circles are for 0.5M and open circles for 0.25M solutions of the 2,3-dimethylbut-2-ene. Solid lines are the results of simultaneous fits to all four data sets to derive rate coefficients for production of HCl(v=0) and HCl(v=1) and for vibrational relaxation of the HCl(v=1) products.

F atom reactions

In the gas phase, F atoms react aggressively and exothermically with alkanes to form vibrationally excited HF. In preliminary experiments, we have succeeded in cleanly generating F atoms in solution and studying the formation of DF products from reaction with deuterated organic molecules on timescales from 1 ps upwards. These experiments are challenging for a number of reasons. Finding a stable precursor that can be photolysed in the UV to release F atoms, yet does not itself attack organic solvents is one example. The considerable width of the DF bands in solution presents further difficulties for product identification and spectroscopic analysis. Results of this work will be presented in a future publication.

Conclusions

The dynamics of chemical reactions in solution in various organic solvents have been observed with vibrational quantum state resolution on timescales of 1 – 1500 ps using transient IR absorption spectroscopy. Exothermic reactions of CN radicals, Cl atoms and F atoms, that are known to channel their available energy into product vibrational excitation for isolated collisions in the gas phase, exhibit similar behaviour in solution. Reaction is followed by vibrational relaxation of the products on timescales as long as a few hundred picoseconds. Our experimental studies, complemented by computer simulation of the reactions, therefore provide insights both into the ways the solvent modifies fundamental mechanisms of chemical reactions, and the interactions between solvent molecules and products in the immediate wake of the reaction. We are able to distinguish solvent caging of reactive events from reaction following diffusion into the bulk liquid medium, and to observe the energy flow between reaction products that are held in close proximity by a solvent cage.

Acknowledgements

The Bristol group gratefully acknowledges funding through the EPSRC Programme Grant EP/G00224X and the ERC Advanced Grant 290966 CAPRI. S.J.G. thanks the EPSRC for a Career Acceleration Fellowship (EP/J002534/1). The ULTRA laser complex at the Central Laser Facility, Rutherford Appleton Laboratory is funded by STFC and BBSRC (STFC Facility Grant ST/501784).

References

1. S.J. Greaves *et al*. Science, **331**, 1423-1426 (2011)
2. R.A. Rose *et al.*, J. Chem. Phys. **134**, 244503 (2011)
3. A.J. Orr-Ewing *et al*., J. Phys. Chem. Lett. **2**, 1139-1144 (2011)
4. D.R. Glowacki *et al*., Nature Chem. **3**, 850-855 (2011)
5. D.R. Glowacki *et al*., J. Chem. Phys. **134**, 314508 (2011)
6. R.A. Rose *et al*., PCCP in press (2012). DOI: 10.1039/C2CP40158D
7. C. Murray and A.J. Orr-Ewing, Int. Rev. Phys. Chem. **23**, 435 –482 (2004)

On the photoelectron spectroscopy of gas-phase polyanions

Contact *j.r.r.verlet@durham.ac.uk*

Jan R. R. Verlet*, Adam S. Chatterley and Daniel A. Horke

Department of Chemistry, University of Durham
South Road, Durham DH1 3LE, U.K.

Introduction

Molecular anions containing more than one excess charge are inherently unstable in the gas-phase due to the strong Coulomb repulsion between the charges. For a polyanion A^{n-}, this would lead to Coulomb explosion (fragmentation) or electron detachment, $A^{(n-1)-} + e^-$. Despite this instability, both these processes have a barrier which arises from a balance between the short range interactions and the long range Coulomb repulsion between the departing charged particle and the remaining anion.[1, 2] This repulsive Coulomb barrier (RCB) can result in a remarkable kinetic stability leading to the formation of exotic species such as polyanions with a negative binding energy.[3] There has been a growing interest in the spectroscopy and dynamics of polyanions both from a fundamental perspective and because in nature, many ions are multiply charged such as in biological systems and in materials.[4-6]

The generation of polyanions in the gas-phase can be conveniently achieved by electrospray ionisation (ESI) and the last decade has witnessed a rapidly growing number of spectroscopic studies on ions produced by ESI. In particular, photoelectron (PE) spectroscopy has emerged as a powerful tool for the study of polyanions as the outgoing PE is sensitive to the RCB.[7] By using PE imaging, angular information about the electron ejection is obtained which can be related to the anisotropic nature of the RCB.[8-10] Most of the work to date has focussed on the spectroscopic properties and as such have primarily employed nanosecond laser sources. In the past few years, our group has demonstrated time-resolved PE imaging of polyanions as a means to studying their excited state dynamics.[11] Excited states provide a route to studying the dynamics of electron tunnelling through the RCB, which in turn provides detailed information about the RCB itself. In this report, the nature of the RCB is considered and its consequence on PE spectroscopy is discussed. In particular, we consider two the effect of internal energy on the RCB.[12]

Experimental

To explore the RCB, we employ the simplest polyanion that exhibits RCBs – dianions. Dye molecules serve ideal test cases to explore the effect of internal energy on the RCB as some possess long-lived fluorescent states that are expected to be sensitive to the RCB. We use the doubly deprotonated fluorescein dianion (Fl^{2-}), see Figure 1(a), which in solution has a quantum yield of 0.92. Fl^{2-} is generated using ESI and injected into a time-of-flight mass-spectrometer before being intersected at the centre of a velocity-map-imaging detector by either tuneable femtosecond (fs) or nanosecond (ns) laser pulses. The former are generated using a commercial amplified Ti:Sapph laser system that is used to pump an optical parametric amplifier, the signal output of which is mixed with the fundamental to yield ~100 fs pulses tuneable from 480 to 535 nm. Nanosecond pulses are generated from a commercial Nd:YAG laser, the 3rd harmonic of which is used to pump and optical parametric oscillator, which is tuneable from 420 nm into the IR.

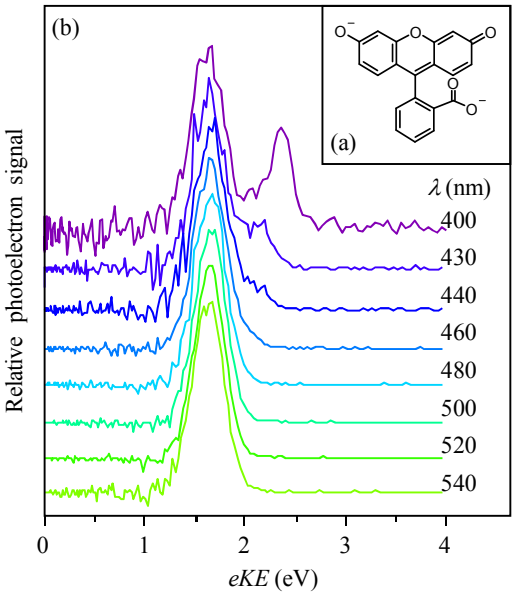

Figure 1: (a) Structure of Fl^{2-}. (b) Photoelectron spectra at various wavelengths resonant with the S_1 excited state of Fl^{2-}.

Effect of internal energy on RCB.

Figure 1(b) shows the PE spectra taken at various wavelengths, resonant with the S_1 state. The lowest energy (540 nm) is close to the 0-0 transition in the gas-phase.[13] The most striking feature of Figure 1(b) is that the PE spectra are identical (in terms of electron kinetic energy, *eKE*) in going from 540 nm to 460 nm. Given that the energy imparted into the system increases by 0.4 eV, one may intuitively expect that such a shift would also be observable in the PE spectrum. Instead, the apparent binding energy of the system is increasing. For wavelengths shorter than 460 nm, an additional feature can be seen at higher *eKE*. As the photon energy increases, this peak shifts as expected in PE spectroscopy. For this peak, the photodetachment is above the RCB and directly into the continuum. In this case, the photoelectron spectrum is determined by the Franck-Condon factors in going from the dianion to the anion.

In order to gain additional insight, we have also measured the excited state dynamics of the S_1 state. Using pump-probe PE spectroscopy (probe at 800 nm), the S_1 state population can be monitored by measuring the integrated photoelectron counts in the feature that arises from the photodetachment of the S_1 state by the probe.[14] The excited state lifetime is measured to be 1.0 ps, as shown in Figure 2. The short lifetime can be assigned to the tunnelling of the electron in the S_1 state through the RCB. Strikingly however, the tunnelling lifetime remains 1.0 ps regardless of excitation wavelength. Because tunnelling is expected to be very sensitive to the width and height of the barrier, our observations strongly suggest that the RCB is not changing as the pump energy is changed.

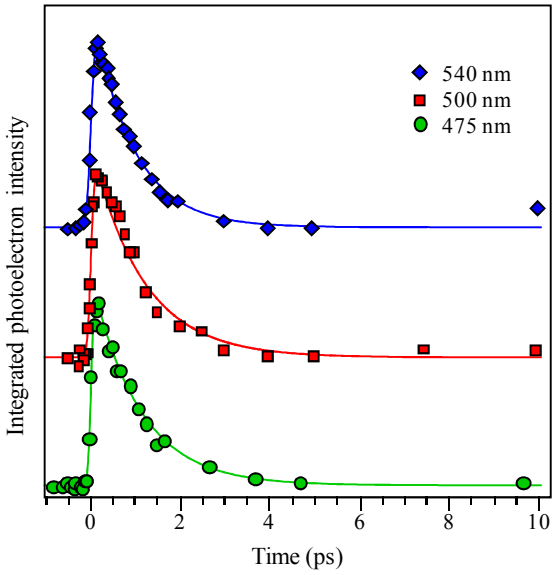

Figure 2: (a) Intgrated photoelectron signal for pump probe signal, reflecting the population of the S_1 state. The observed dynamics can be correlated with electron tunnelling through the repulsive Coulomb barrier.

In order to explain these observations, we consider the effect of introducing additional internal energy into the system as the photon energy is increased. If we assume that the electron dynamics can be decoupled from the nuclear dynamics, then electron loss through tunnelling is expected to lead to a conservation of the internal energy imparted in the S_1 excitation. This accounts for the PE spectra in Figure 1(b): as the asymptotic ε is the same and the additional energy has gone into the internal modes of the Fl^- product. As a result, the RCB height as viewed from the $Fl^- + e^-$ asymptote will remain the same and consequently, the electron will observe the same RCB and thus, will tunnel at the same rate through this barrier. At wavelengths below 460 nm, there is a competition between direct over-the-barrier detachment and tunnelling. Interestingly, the tunnelling remains an important channel despite the fact that the total energy is sufficient to directly remove the electron.

Conclusions

We have observed that the electron tunnelling through the RCB in Fl^{2-} is strongly adiabatic. This is likely to be a general feature of polyanions and consequently will have profound implications on the interpretation of the PE spectra of such systems. For example, there have been a number of PE spectroscopy experiments in recent years on oligonucleotides with photodetachment lasers operating at 266 and 213 nm.[15] These energies are resonant with the bright ππ* states of the bases which may be bound solely by the RCB. In such cases, the PE spectrum must be interpreted with extreme caution as the observed PE spectrum is not the usual vertical transition that is solely dependent on the Franck-Condon overlap.

Acknowledgements

We thank the laser loan pool facility of the STFC Central Laser Facility for loan of the Nd:YAG laser system. This work has been supported by the EPSRC (EP/D073472/1) and Durham University. ASC is funded by the Leverhulme Trust.

References

[1] Wang, et al, *Phys Rev Lett* **81**, 2667 (1998)
[2] Wang, et al, *Phys Rev Lett* **81**, 3351 (1998)
[3] Wang, et al, *Nature* **400**, 245 (1999)
[4] Scheller, et al, *Science* **270**, 1160 (1995)
[5] Boldyrev, et al, *Acc Chem Res* **29**, 497 (1996)
[6] Dreuw, et al, *Chem Rev* **102**, 181 (2002)
[7] Wang, et al, in *Annu Rev Phys Chem* (2009), Vol. 60, pp. 105.
[8] Xing, et al, *J Chem Phys* **130** (2009)
[9] Xing, et al, *J Phys Chem A* **113**, 945 (2009)
[10] Horke, et al, *Journal of Physical Chemistry Letters* **3**, 834 (2012)
[11] Lecointre, et al, *J Phys Chem A* **114**, 11216 (2010)
[12] Horke, et al, *Phys Rev Lett* **108** (2012)
[13] McQueen, et al, *Angewandte Chemie-International Edition* **49**, 9193 (2010)
[14] Verlet, *Chem Soc Rev* **37**, 505 (2008)
[15] For example: Yang, et al, *Proc Natl Acad Sci U S A* **101**, 17588 (2004)